Earth and Planetary Science Letters 593 (2022) 117686

Contents lists available at ScienceDirect

Earth and Planetary Science Letters

www.elsevier.com/locate/epsl

Crustal structure and subsidence mechanisms of the Williston Basin: New constraints from receiver function imaging

Jianguo Song [a,b], Stephen S. Gao [b,*], Kelly H. Liu [b], Muchen Sun [b,c], Youqiang Yu [b,c], Fansheng Kong [b,d], Kevin Mickus [e]

[a] College of Geosciences, China University of Petroleum, Qingdao, Shandong, China
[b] Geology and Geophysics Program, Missouri University of Science and Technology, Rolla, MO, USA
[c] State Key Laboratory of Marine Geology, Tongji University, Shanghai, China
[d] Key Laboratory of Submarine Geosciences, Second Institute of Oceanography, Ministry of Natural Resources, Hangzhou, China
[e] Department of Geography, Geology, and Planning, Missouri State University, Springfield, MO, USA

ARTICLE INFO

Article history:
Received 1 November 2021
Received in revised form 17 May 2022
Accepted 17 June 2022
Available online xxxx
Editor: H. Thybo

Dataset link: https://ds.iris.edu/ds/nodes/dmc

Dataset link: https://doi.org/10.7914/SN/CN

Dataset link: https://doi.org/10.7914/SN/IU

Dataset link: https://doi.org/10.7914/SN/N4

Dataset link: https://doi.org/10.7914/SN/TA

Dataset link: https://doi.org/10.7914/SN/US

Dataset link: https://doi.org/10.7914/SN/WY

Dataset link: https://doi.org/10.7914/SN/X6_2014

Dataset link: https://doi.org/10.7914/SN/XC_2000

Dataset link: https://doi.org/10.7914/SN/XI_2011

Dataset link: https://doi.org/10.7914/SN/XR_2001

Dataset link: https://doi.org/10.7914/SN/XS_1999

Dataset link: https://doi.org/10.7914/SN/XV_2009

Dataset link: https://doi.org/10.7914/SN/YB_1996

Keywords:
Williston Basin

ABSTRACT

Mechanisms responsible for the long-term subsidence of intracontinental basins such as the Williston Basin in North America remain enigmatic, partly due to the thick sedimentary layer commonly found in the basins that prevents reliably imaging the deep crustal and upper mantle structures using some of the most-commonly employed seismic methods such as receiver function analysis. In this study, we used receiver functions recorded by 274 USArray and other stations in the Williston Basin and adjacent areas to investigate the layered structure of the crust in the hydrocarbon-rich intracontinental basin. After the removal of strong reverberations on the receiver functions associated with a low-velocity sedimentary layer using a recently developed time-domain deconvolution approach, two positive arrivals representing downward increases of seismic velocities are imaged beneath the basin and the area to the west. The top interface has a depth of about 40 km at the depocenter of the basin, and gradually shallows eastward to about 30 km beneath the Superior Craton, and the deeper interface has a mean depth of about 65 km beneath the Williston Basin. The layer between the two interfaces may represent an eclogitized or garnet-rich lower crustal layer. The results are consistent with the hypothesis that continuous retrograde metamorphic reactions in the previously-thickened lower crust during the Paleoproterozoic Trans-Hudson Orogeny resulted in the subsidence of the intracontinental Williston Basin.

* Corresponding author.
E-mail address: sgao@mst.edu (S.S. Gao).

https://doi.org/10.1016/j.epsl.2022.117686
0012-821X/

Superior Craton
crustal structure
receiver function
Wyoming craton
receiver functions

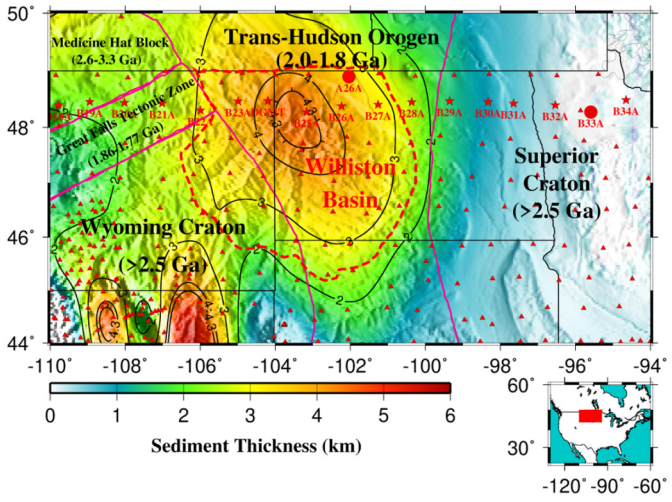

Fig. 1. Distribution of seismic stations (triangles) and major tectonic features (Foster et al., 2006) of the study area. The background image shows the thickness of Phanerozoic sediments (Laske and Masters, 1997). The two red dots denote the two stations (A26A and B33A) used in Fig. 3, and the 17 red stars represent stations used in Figs. S4-S20 to demonstrate the effectiveness of the reverberation removal procedure. The region shaded in red in the inset map of North America shows the study area. (For interpretation of the colors in the figure(s), the reader is referred to the web version of this article.)

1. Introduction

The Williston Basin (WB) of the north-central United States and southern Canada (Fig. 1) is the archetype of intracontinental basins, with an elliptical shape and subsidence episodes that spanned a 400 million year period from the Cambrian to Jurassic (Kent and Christopher, 1994). While the basin is considered an intracontinental basin, it initially started as a cratonic margin basin as Upper Cambrian strata were deposited on the edge of the western craton embayment (Burgess, 2008). As material accreted to the western United States during various Paleozoic and Mesozoic orogenic events, it slowly became an intracontinental basin. The establishment of the current elliptical shape of the WB started in the Devonian and was completed by the Cretaceous Laramide orogeny (Kent and Christopher, 1994).

The Phanerozoic sedimentary layer at the depocenter of the basin reaches a maximum thickness of about 4.5 km (Fig. 1; Laske and Masters, 1997). While all periods between the Cambrian and Jurassic are represented, the sediments were deposited in five depositional intervals with distinctive unconformities between these events (Kent and Christopher, 1994). The basin is largely centered over the lithologies of the Trans-Hudson Orogen (THO), a Paleoproterozoic collisional belt between the Superior and Wyoming cratons developed between 2.0 and 1.8 Ga (Green et al., 1985). Based on gravity and magnetic studies (Green et al., 1985), seismic reflection profiling (Baird et al., 1995) and scattered deep drill holes (Kent and Christopher, 1994), the basement underlying the WB includes three Proterozoic terranes: 1) Archean Wyoming and Hearn Cratons to the west, 2) THO in the center, and 3) the Superior Craton to the east. Although the basin is generally considered an intracontinental basin, the surface of the Archean and Proterozoic basement is far from being smooth as seismic reflection profiling and drill hole data identified at least ten large scale structure features (e.g., domes) and basin-wide faults within the basement (Kent and Christopher, 1994; Burgess, 2008).

Partly because the WB is a major oil and gas producer in the U.S. and one of the four major shale oil plays in the country, numerous geological and geophysical investigations have been conducted over the past several decades, mostly targeting the top several kilometers. A number of contrasting models have been proposed to explain the basin's characteristic tectonic features and subsidence history. These models involve thermal, magmatic, metamorphic, extraterrestrial impact, and kinematic processes in the crust, mantle lithosphere, and asthenosphere (Beaumont, 1978; Jarvis and McKenzie, 1980; Quinlan, 1987; Middleton, 1989; Sears and Alt, 1992; Baird et al., 1995; Naimark and Ismail-Zadeh, 1995; Allen and Armitage, 2012; Daly et al., 2018; Watts et al., 2018). One of the most commonly-invoked models attributes the long-term subsidence of intracontinental basins such as the WB to continuous formation of garnet or eclogite in the lower crust (Green and Ringwood, 1967; Fowler and Nisbet, 1985; Kay and Kay, 1991; Hamdani et al., 1994; Baird et al., 1995; Fischer, 2002; Gac et al., 2013; Schulte-Pelkum et al., 2017). Cooling of the thickened lower crust beneath collisional belts such as the THO may promote garnet growth, and consequently form a dense lower crustal layer characterized by a P-velocity greater than 7.0 km/s (i.e., the 7.x layer). The formation of a garnet or eclogite layer is usually attributed to some type of tectonic event or the aftermath of such an event that involved the upper mantle and lower crust (Artyushkov and Baer, 1983; Allen and Armitage, 2012). However, models attributing the formation of the WB to Proterozoic events cannot satisfactorily explain the significant time gap between the THO and the first sediments (Upper Cambrian) in the WB.

In the contiguous U.S., the 7.x layer has been detected through seismic refraction, surface wave tomography, and receiver function (RF) studies beneath the Rocky Mountains, the eastern half of the Great Plains of North America, and most of the eastern U.S. (e.g., see Fig. 2 of Schulte-Pelkum et al., 2017). The existence of a 7.x layer beneath the WB and most other areas covered by a layer of low-velocity Phanerozoic sediments is ambiguous and debated, especially among studies using receiver functions (RFs) (e.g., Thurner et al., 2015; Schulte-Pelkum et al., 2017). Such uncertainties are largely due to the strong reverberations in the RFs associated with the sedimentary layer and the resulting possibility of misidentifying one of the pulses in the reverberation series as the Moho. Higher than normal shear velocities have been suggested beneath the WB from surface wave tomographic studies (Schmandt et al., 2015; Shen and Ritzwoller, 2016), but whether they represent the 7.x layer is not clear.

In this study, by applying a frequency-domain deconvolution technique that we recently developed (Yu et al., 2015) to remove the sedimentary reverberations from the RFs, the existence of a lower crustal layer with a thickness up to 25 km is revealed beneath the WB. Our results suggest that cooling-induced densification of this lower crustal layer through garnet growth or eclogitization can explain the long-term subsidence of the WB.

2. Data and methods

2.1. Data and RF calculation

The broadband seismic data used in this study were obtained from the Data Management Center (DMC) of the Incorporated Re-

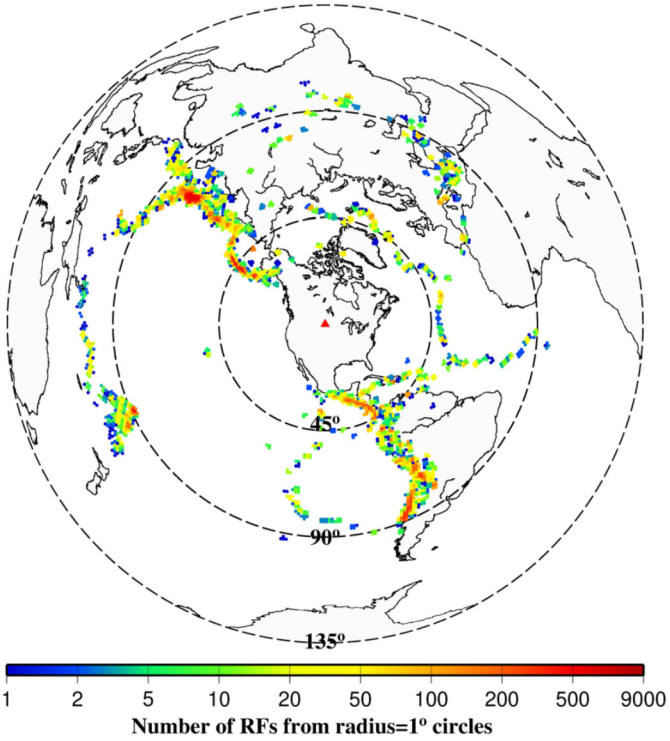

Fig. 2. An azimuthal equidistant map centered at the approximate center (red triangle) of the study area showing earthquake source areas. Each dot represents a radius = 1° circular bin. The distance between neighboring bins is 1°. The color represents the number of used receiver functions originated from earthquakes in the bins. The distance (in degrees) from the center of the study area is indicated by the number on the circles.

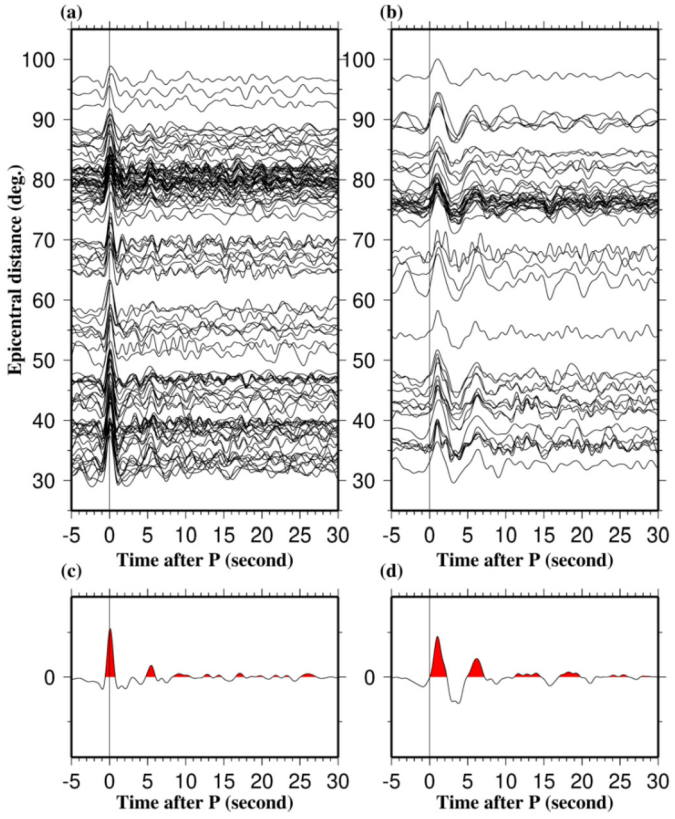

Fig. 3. RFs recorded by (a) Station B33A located on the Superior Craton, and (b) Station A26A in the WB plotted against the epicentral distance. (c) and (d) are simple time-domain summations of the RFs shown in (a) and (b), respectively.

search Institutions for Seismology (IRIS), recorded over the period from July, 1996 to March, 2022. Most of the data were recorded by stations belonging to the EarthScope Transportable Array (TA) of the EarthScope Initiative, which covered the study area during the period of 2007-2012. The epicentral distances range from 30° to 100°, and the cutoff earthquake magnitude used for data request was computed using an empirical formula that considers the focal depth and the epicentral distance to balance the quantity and the quality of the requested data (Liu and Gao, 2010). The three-component seismograms were windowed 10 s before and 100 s after the theoretical arrival time of the first P-wave, and were bandpass filtered in the frequency range of 0.1-1.0 Hz. Filtered seismograms with robust P arrivals on the vertical component were then converted into radial RFs using the water-level deconvolution approach (Ammon, 1991). The water-level and Gaussian width values used for computing the RFs are 0.03 and 5.0 (which corresponds to a low-pass frequency of 2.4 Hz), respectively. Totally 27544 RFs from 2608 teleseismic events (Fig. 2) were used for the study. The number of seismic stations is 274 (Fig. 1), including 148 EarthScope TA stations. To estimate the sharpness of the discontinuities which is quantified by the thickness of the gradient transition, the seismograms were also filtered in several frequency bands with corner frequencies f_1 and 2.4 Hz, where $f_1 = 0.08$, 0.12, 0.16, and 0.20 Hz, prior to conversion to RFs.

2.2. Removal of reverberations associated with a low-velocity sedimentary layer

Fig. 3 shows RFs recorded by two different stations. While the RFs recorded by TA station B33A, which was located on the Superior Craton outside the WB, have a simple waveform that is typical for RFs obtained at stations deployed on basement rocks, the RFs from TA station A26A, which was in the WB, show a peak that is delayed by about 1 s. Additionally, the waveforms are dominated by a decaying series of reverberations with a period of about 5 s. Those features are characteristics of shear wave multiple reflections in a low-velocity layer of unconsolidated or partially consolidated sediments (Yu et al., 2015). The first peak is termed Pbs by Yu et al. (2015), which is the P-to-S conversion from the bottom of the low-velocity sedimentary layer, and its delay time is proportional to the thickness of the layer. Figs. S1-S3 show three additional station pairs located in the northeastern corner of the study area to demonstrate the pervasiveness of the sharp contrast of the waveforms between basin and cratonic stations.

The reverberations can be effectively removed by applying a frequency-domain deconvolution procedure that utilizes a reflection coefficient and the period of the reverberations (Fig. 3b), both of which can be measured from the auto-correlation function of the RFs (Yu et al., 2015). To demonstrate the effectiveness of the reverberation-removal procedure, we produced a synthetic RF attempting to match the RFs recorded at Station B22A, using a reflectivity-based procedure (Randall, 1994). In order to maximize the similarity between the recorded and calculated RFs, we tried a number of different models and the optimal model has 4 layers, which are separated by the bottom of the low-velocity sedimentary layer, an intracrustal interface, and the Moho (Table S1). For a surface event with an epicentral distance of 65°, the predicted arrival times of the P-to-S converted phase from the base of the sedimentary layer, the intracrustal interface, and the Moho are 0.83, 5.65, and 7.85 s, respectively. The three arrivals are respectively labeled as Pbs, Pis, and Pms in Fig. 4. We acknowledge that different combinations of parameters in the model may lead to a similar goodness of fit between the calculated and recorded RFs, but the low velocity sedimentary layer, an intracrustal interface,

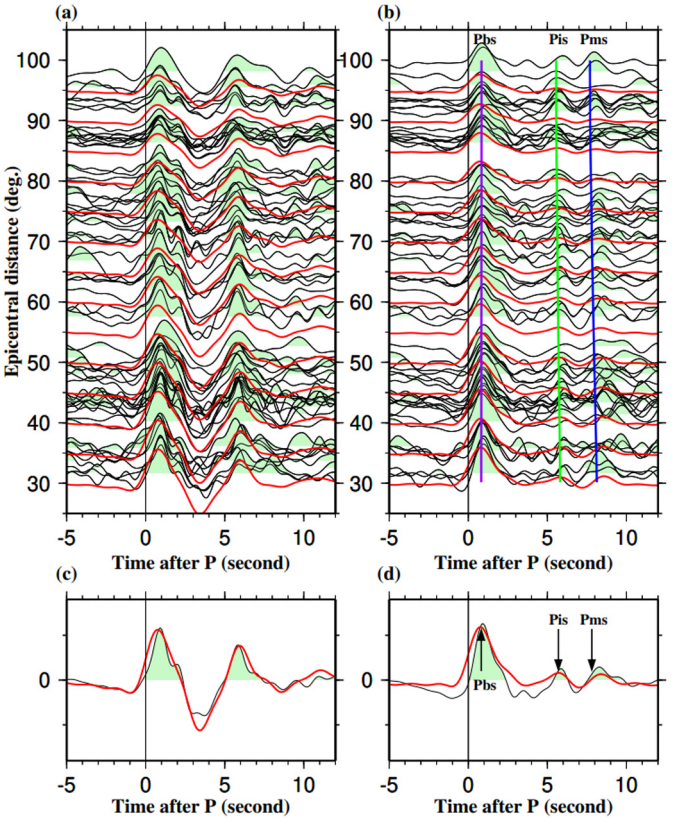

Fig. 4. (a) RFs recorded by station B22A in the WB (black traces) and synthetic RFs obtained at an epicentral distance interval of 5° (red traces). (b) Same as those shown in (a) but after applying the reverberation-removal procedure. The purple, green and blue lines mark the onset times of the Pbs, Pis, and Pms arrivals, respectively. (c) and (d) are simple time-domain summations of the RFs shown in (a) and (b), respectively. Pbs: P-to-S conversion from the base of the loose sedimentary layer; Pis: P-to-S conversion from an intracrustal layer; Pms: P-to-S conversion from the Moho. Note that the arrows point to the theoretical onset rather than the peak of the arrivals.

and the Moho are required in order to match the major characteristics of the original and reverberation-removed RFs.

The resulting synthetic RFs (red traces in Fig. 4a) capture all the major characteristics of the recorded ones, especially the amount of shift of the first positive peak, and the periods and amplitudes of the waveform (Figs. 4a and 4c). Such similarities are best observed on the stacked traces (Fig. 4c). After the application of the reverberation removal filter to both the recorded (black traces in Fig. 4b) and synthetic (red traces in Fig. 4b) RFs, the multiples are largely removed, and the resultant synthetic reverberation-free RFs match the observed ones reasonably well (Figs. 4b and 4d). The arrival times of the three most prominent peaks on the reverberation-removed synthetic RFs agree with the predicted arrival times and polarity of the Pbs, Pis, and Pms arrivals (Fig. 4d, red trace), and thus they are unlikely to be artifacts produced by the reverberation-removal process. The fact that the three peaks can also be observed on the recorded RFs at approximately the same times as those on the synthetic RFs suggests that the reverberation-removal procedure also performed well on the recorded RFs (Fig. 4d, black trace).

To provide additional demonstration on the effectiveness of the reverberation-removal procedure, the original and processed RFs for each of the 17 USArray-TA Profile "B" stations (in the approximate latitudinal range of 48°-48.5°, Fig. 1) are displayed in Figs. S4-S20. The reverberations on the processed RFs at stations in the WB are clearly reduced.

2.3. Receiver function stacking

To produce E-W profiles of stacked RFs, we divided the top 100 km of the Earth within the study area into rectangular blocks of $1° \times 1° \times 1$ km (N-S, E-W, and vertical) with E-W and vertical moving steps of 0.1° and 0.1 km, respectively. We then ray-traced the RFs and computed the mean amplitude of the RFs in each of the blocks. The ray-tracing is performed using a velocity model composed of a mean crustal Vp (Vs) of 6.1 (3.39) km/s. The IASP91 Earth model was used for sub-crustal velocities and structure to compute the ray parameters. The stacked RFs are normalized by the maximum amplitude in the 30-75 km depth range. The procedure is similar to common conversion point (CCP) stacking (Dueker and Sheehan, 1997). A total of five E-W profiles, which are centered at 45-49° N with an interval of 1°, were produced. With an estimated upper limit of 5% of uncertainty in the mean crustal velocities, the depths of the resulting interfaces (including an intracrustal interface and the Moho) may have an uncertainty of no more than 4 km, as determined by synthetic tests (Nair et al., 2006). In particular, the crustal thickness in the area with the greatest sedimentary thickness is overestimated by a few kilometers. As demonstrated below, this uncertainty has negligible effects on the main conclusions of the study, which are mostly drawn from the existence of the interfaces and their lateral depth variations rather than the absolute depths. The depths of the Pis and Pms phases are manually picked by taking considerations of the robustness of the arrivals, and the similarity of both the waveforms and depths with neighboring bins.

3. Results

3.1. Effects of the low-velocity sedimentary layer atop the Williston Basin on the RFs

The existence of a low-velocity sedimentary layer in the WB and the area to the west is unambiguously indicated by the strong reverberations observed in the RFs (e.g., Figs. 3b and 5b), and by the systematic spatial variation of up to 1.5 s delay of the first peak on the RFs (Fig. 6). The largest delay of the first peak is found at the depocenter of the WB, where the Phanerozoic sediments are the thickest (Fig. 1). A clear correlation between the delay times (Fig. 6) and the sediment thickness (Fig. 1) is revealed (Fig. 7). The delay times increase more rapidly for smaller thickness (Fig. 7) in response to the lower velocities. The change in the slope occurs at about 1.5 km, which is probably the boundary between the low-velocity sedimentary layer and consolidated Phanerozoic sedimentary rocks. The estimated thickness of the low-velocity sedimentary layer is consistent with the model used for producing the synthetic RFs (Table S1).

Fig. 5 shows cross sections of the stacked original and reverberation-removed RFs along an E-W profile centered at 49°N. Similar cross sections for the other four E-W profiles centered at 45-48°N can be found in Figs. S21-S24, and those for all the 15 N-S profiles can be found at Figs. S25-S39. Strong reverberations are observed on the stacked RFs beneath the WB on the profiles created using the pre-reverberation-removed RFs (Fig. 5b). The wavelength of the reverberations (white vertical wiggles in Fig. 5b) increases in areas with thicker Phanerozoic sediments (Fig. 5a). Due to the unfortunate fact that the depth of the second positive arrival (~30-40 km) is comparable to the expected depth of the Moho beneath stable continental areas, this arrival in the reverberating series (Fig. 5b) can easily be mis-identified as the P-to-S conversion from the Moho or a subducted continental slab.

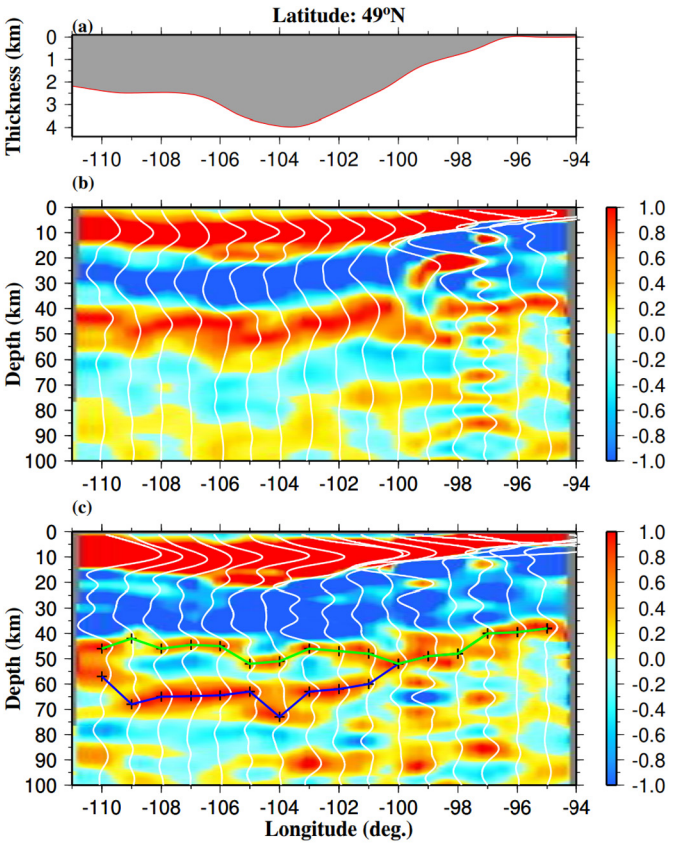

Fig. 5. Results of stacking migrated RFs in a 1-degree-wide E-W band centered at 49°N latitudinal line. (a) Thickness of Phanerozoic sediments in km. (b) Migrated original RFs. (c) Migrated reverberation-removed RFs. Pluses indicate the hand-picked Moho doublet. The green curve marks the shallower interface, and the blue curve shows the deeper interface. The scale bar in (b) and (c) shows stacking amplitudes normalized by the maximum amplitude in the depth range of 30-75 km in the bins.

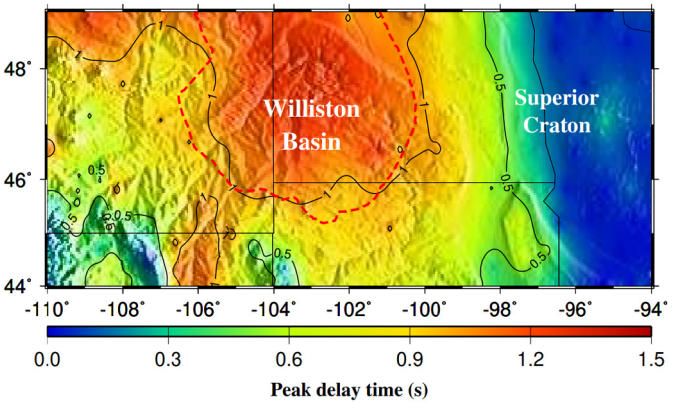

Fig. 6. Distribution of delay time of the first positive peak on the RFs.

3.2. Crustal thickness beneath the Superior Craton

On the cross sections produced using both the original (e.g., Fig. 5b) and reverberation-removed (Fig. 5c) RFs, a prominent positive arrival is observed at the depth of 30-45 km beneath the Superior Craton (Fig. 8), where a low-velocity sedimentary layer is absent and thus the RFs are not contaminated by the reverberations. The amplitude of this arrival relative to that of the direct P-wave is about 0.05, which is about half of that observed on the stable portions of the Archean Kaapvaal and Zimbabwe cratons (Nair et al., 2006). Because this is the only continuous positive interface in the expected depth range of the petrological Moho under this area (Baird et al., 1995), we consider it to be the Moho. The agreement on crustal thickness between results from this study and previous active source seismic studies (e.g., Baird et al., 1995) indicates the reliability of the techniques that we utilized in the study.

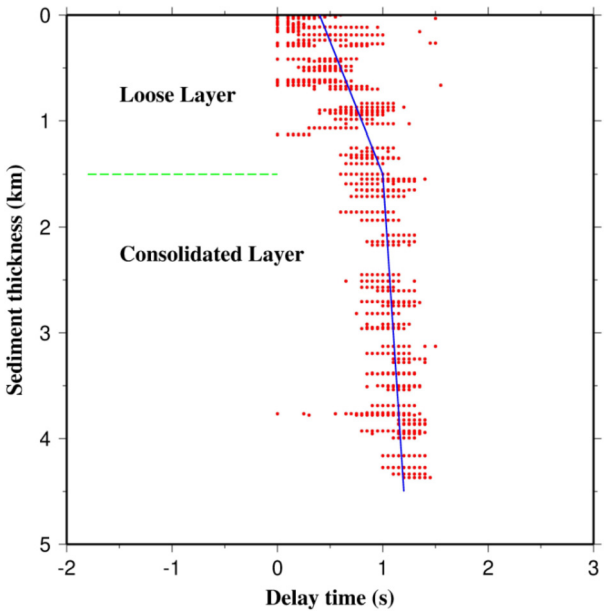

Fig. 7. A cross plot of sedimentary layer thicknesses shown in Fig. 1 and the delay times of the first peak on the RFs shown in Fig. 6. The solid blue lines are results of best-fitting, and the dashed green line separates the loose and consolidated layers.

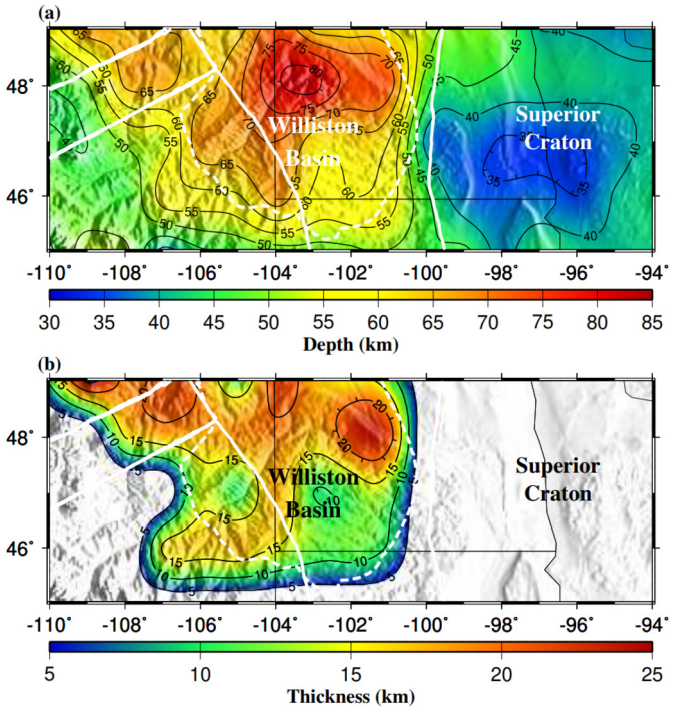

Fig. 8. (a) Resulting depth to the lower interface which is considered to be the petrological Moho. (b) Thickness of the lower crustal layer between the two interfaces.

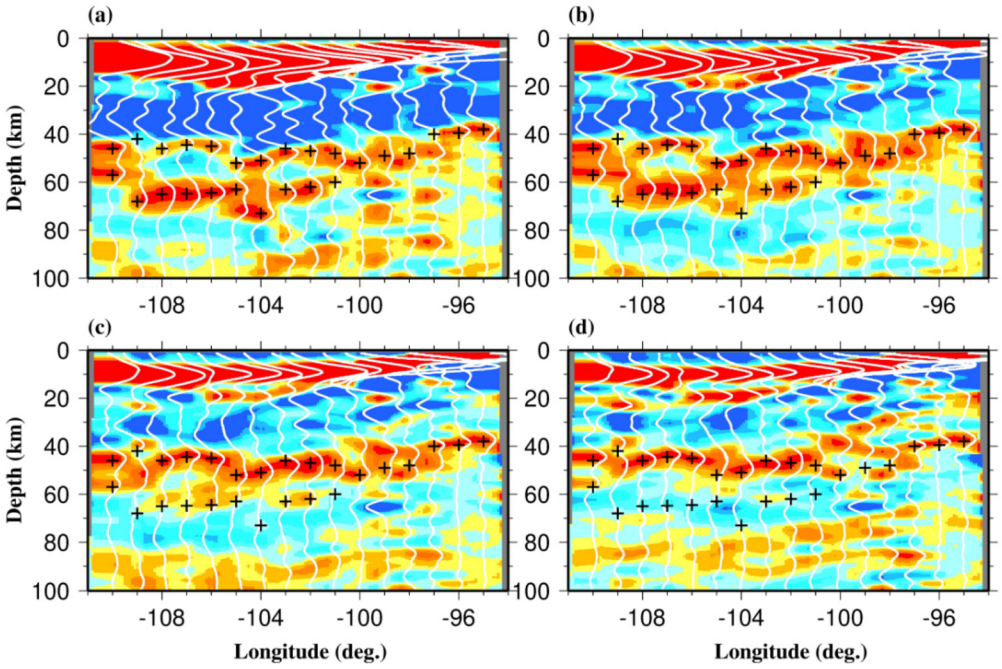

Fig. 9. Same as Fig. 5c but for different bandpass filtering corner frequencies. (a) 0.08-2.4 Hz; (b) 0.12-2.4 Hz; (c) 0.16-2.4 Hz; (d) 0.20-2.4 Hz. Note that for the purpose of comparison, the Pis and Pms arrivals obtained in the frequency band of 0.1-1.0 Hz (Fig. 5c) are plotted as pluses.

3.3. Crustal layering beneath the WB and the areas to the west

The WB and the neighboring areas to the west, which are covered by Phanerozoic sediments (Fig. 1), are characterized by a Moho doublet structure that is observed on the reverberation-removed RF profiles (e.g., Figs. 5c and S21-S23). The deeper interface, which is likely the petrological Moho (O'Reilly and Griffin, 2013), has a depth ranging from about 50 to 80 km with a mean value of about 65 km beneath the WB, and the shallower one has a depth of 40-55 km (Fig. 8). In general, the thickness of the layer between the two interfaces is greater for areas with a thicker sedimentary layer (Figs. 1 and 8b). This correspondence may suggest a possible causal relation between basin subsidence and crustal layering, as discussed below.

4. Discussion

4.1. Comparison with previous studies

The existence of a high velocity lower crustal layer beneath the WB has been suggested based on data from COCORP and Lithoprobe seismic reflection experiments (see summaries in Baird et al., 1995), which have a limited spatial coverage in the study area. Beneath the Superior Craton portion of the study area, our crustal thickness results agree well with those reported by Thurner et al. (2015) who imaged crustal structure using RFs from approximately the same stations. However, the thicknesses from the two studies are significantly different for the rest of the study area where a low-velocity sedimentary layer is present. The difference is most likely caused by a possible misidentification of the second positive pulse on the sedimentary multiple series as the P-to-S conversion from the Moho, a possibility that has also been suggested by Schulte-Pelkum et al. (2017). The high degree of similarity between the cross sections produced using the original (pre-reverberation-removal) RFs (e.g., Figs. 5b) and those presented in Thurner et al. (2015) further confirms this possibility.

The existence of a high velocity layer in the lower crust is consistent with recent surface wave tomographic results. For instance, in the contiguous U.S., Schmandt et al. (2015) revealed that one of the two areas with the highest shear velocities in the lowest 11 km of the crust is the WB and the region to its immediate west. This pattern is similar to the results of Shen and Ritzwoller (2016) for velocities in the bottom 3 km thickness layer above the Moho. In addition, Shen and Ritzwoller (2016) found that the WB and surrounding areas possess the thickest high-velocity lower-crustal layer (up to 15 km thick with a shear velocity of 4.0 km/s or greater) in the entire contiguous U.S.

4.2. Frequency dependence of the RFs

It has long been recognized that crustal and mantle discontinuities have a finite "sharpness" that can be quantified as the thickness of the layer with a seismic impedance gradient (Benz and Vidale, 1993; Bostock, 1999). In order for a discontinuity to be observed using P-to-S conversions, the thickness should be less than approximately half of the wavelength (λ) of the P wave (Bostock, 1999). We filtered the original seismograms in 4 different frequency bands with corner frequencies of $f_1 = 0.08+(i-1)*0.04$ Hz (where $i = 1, 2, 3, 4$) and $f_2 = 2.4$ Hz, computed the RFs and performed the stacking using the same parameters that we used for producing the results shown in Fig. 5. If we assume a Vp of 7.2 km/s, the discontinuity cannot be detected if the thickness of the transitional layer is greater than 45, 30, 23, and 18 km for $f_1 = 0.08$ ($\lambda = 90$ km), 0.12 ($\lambda = 60$ km), 0.16 ($\lambda = 45$ km), and 0.20 ($\lambda = 36$ km) Hz, respectively. The results (Fig. 9) indicate that the interface at ~40 km beneath both the WB and the Superior Craton can be consistently observed at all the frequencies, suggesting that it is a sharp boundary with a gradient thickness of 18 km or less that is characteristic of a "normal" Moho discontinuity. In contrast, the deeper interface at ~60 km beneath the WB is barely observable for $f_1 = 0.16$ Hz (Fig. 9c) and non-observable for $f_1 = 0.20$ Hz (Fig. 9d), indicating that the interface must have a gradient thickness of 18-23 km or greater. Such a gradual Moho may be attributed to eclogitization of the thickened lower crust (e.g., Bascou et al., 2001; Wittlinger et al., 2009).

4.3. Constraints on subsidence models

A number of models have been proposed to explain the long-term subsidence of intracontinental basins including the WB. The anomalously thick crust beneath the WB is inconsistent with the thermal contraction model (Sleep and Snell, 1976), which predicts a normal crustal thickness and an exponential rather than linear rate of subsidence (Baird et al., 1995). The thick crust and the existence of the high velocity lower crustal layer are also not in agreement with the crustal properties predicted by lithospheric necking (Armitage and Allen, 2010) which would result in a thinner than normal crust beneath the WB.

Recent studies combining seismic reflection and gravity data for the Parnaiba, Michigan, and Congo basins (Daly et al., 2018; Watts et al., 2018) have confirmed the presence of a 7.x layer immediately above the Moho. Mostly on the basis of the existence of a linear gravity maximum observed after the removal of the gravity effect of the sedimentary layers, these studies favor a model of subsidence resulting from cooling of mantle-derived igneous material through dyking and basal underplating (Daly et al., 2018). The observed high velocity lower crustal layer beneath the WB, which developed in an existing orogenic belt (the THO), is several times thicker than that observed for basins that developed on thick continental lithosphere (Watts et al., 2018). Additionally, while the subsidence rate of the basins is exponential which is consistent with thermal contraction (Sleep and Snell, 1976; Watts et al., 2018), that of the WB is mostly linear (Baird et al., 1995).

Results from this study for the WB are consistent with the continuous phase transition model of intracontinental basins (Haxby et al., 1976; Kaus et al., 2005). It has been established that tectonic over-thickening of the crust can lead to the phase transition from gabbro (density = 3 g/cm^3, Vp = 6.9 km/s) to eclogite (density = 3.5 g/cm^3, Vp = 7.9-8.05 km/s) in the lower crust (e.g., Artyushkov and Baer, 1983; Kay and Kay, 1991; Kern et al., 1999). The area with the thickest lower crustal layer in the WB is approximately consistent with the area with the maximum Bouguer gravity anomaly after removing the gravitational effects of the sediments (Mickus, 2007), an observation that provides independent evidence for the existence of a high density lower crustal layer in the WB.

Because the acoustic impedance for pure eclogite is higher than that of the upper-most mantle, the fact that a positive contrast in impedance from the crust to the mantle is observed beneath the WB suggests partial rather than full gabbro-eclogite transition. Partial gabbro-eclogite transition has been invoked by some previous studies to explain the subsidence of the Williston and other intracontinental basins (e.g., Haxby et al., 1976; Fowler and Nisbet, 1985; Kaus et al., 2005). Gabbro-eclogite transition can take place under normal crustal geothermal conditions if the crust is thicker than 50 km (Fowler and Nisbet, 1985; Kay and Kay, 1991), a threshold value that is pervasively observed beneath collisional belts such as the THO. In addition to eclogitization, garnet growth within a granulite facies in response to the decrease in crustal temperature after the ceasing of a collisional event can also increase the density of the crust (Fischer, 2002). Such retrograde metamorphism has also been proposed for the formation of the 7.x layer observed in the lower-most part of the crust beneath the Rocky Mountains and the central and eastern U.S. (Rumpfhuber and Keller, 2009; Keller, 2013; Schulte-Pelkum et al., 2017). Similarly, beneath the Tibetan Plateau, an ~20 km thick high density, high velocity layer in the depth range of ~63-83 km was suggested to be eclogitic (Wittlinger et al., 2009).

Long-term cooling induced retrograde metamorphic reactions in the lower crust, mainly garnet growth and gabbro eclogitization (Bousquet et al., 1997), have been utilized to explain the progressive reduction of the ratio between surface relief and crust root magnitude beneath collisional mountains (Fischer, 2002). Gabbro-eclogite transformation was proposed to be responsible for continental crust subsidence in old fold belts such as the Urals and Appalachians (Artyushkov and Baer, 1983). The ratio approaches zero for Proterozoic collisional zones due to the progressive erosion of the mountain belt and the consequent uplift of the Moho (Fischer, 2002). Our observations suggest that under some circumstances, the rate of mass increase due to eclogitization or garnet growth in the lower crust may exceed that of the mass decrease at the surface from erosion. Consequently, the bottom of the crust subsides rather than uplifts in order to maintain isostatic equilibrium, leading to the formation of intracontinental basins above the thickened crust (Bousquet et al., 1997). Density increase of the lower crust has also been suggested in modern rift zones through magmatic intrusion (Thybo and Nielsen, 2009).

Although the existence of a high density lower crustal layer developed in the over-thickened crust of the THO can explain the long-term linear subsidence of the WB, the question of why the basin formed in this particular segment of the THO remains unanswered. Some previous studies attributed this to the fact that the WB is in the narrowest section of the THO where the maximum crustal shortening might have occurred (Baird et al., 1995). The reason for its near circular shape instead of being elongated along the THO is equally puzzling. We speculate that a possible mechanism for the circular shape is a positive feedback between subsidence and densification metamorphism, i.e., once eclogitization and/or garnet growth reactions have started in a localized area, subsidence of this area leads to an accelerated rate of metamorphism, which further enhances subsidence. Alternatively, the area that subsided could be seated on a passing mantle plume, which might have induced eclogitization in the deformed crust in the THO and led to subsidence, a process that has been proposed for the two-phase rifting of the New Madrid Seismic Zone in the central U.S. (Cox and Van Arsdale, 2002). In addition, a plume can produce an underplated layer beneath the original Moho, forming a high velocity lower crust. This mechanism has been proposed for the Midcontinent Rift which is located to the east of the study area (Zhang et al., 2016). Under this model, the Pis phase discussed above would represent the original (pre-underplating) Moho, and the Pms phase would reflect the bottom of the underplated layer.

4.4. Low mantle density beneath the thin crust of the Superior Craton

The portion of the Superior Craton adjacent to the THO is underlain by a crust with a minimum thickness of approx. 30 km, which is anomalously thin for crust in stable cratonic areas. This area of thin crust is also observed by Thurner et al. (2015) and several other studies of different spatial scale (e.g., Laske and Masters, 1997; Frederiksen and Delaney, 2015). Further to the east, the crust beneath the Superior Craton near the western boundary of the Midcontinent rift is about 35-40 km (Zhang et al., 2016) which is normal to other typical continental areas. While an in-depth investigation of the causes of this anomalously thin crust is beyond the scope of this study, which is focused on the WB, simple calculations based on Airy's hypothesis of isostasy suggest that the crust beneath this area must be underlain by a low-density upper mantle. The amount of predicted mantle density reduction is a function of the thickness of the anomalous mantle layer. A regional seismic tomography study (Bollmann et al., 2019) suggests a low velocity zone extending to the depth of ~200 km beneath this area. Under the assumption that this low velocity feature also has a low density, the estimated density anomaly is about −0.8%. The lower density and corresponding lower velocities in the uppermost mantle are consistent with the observed small amplitudes of the P-to-S conversions from the Moho in this area relative to

other typical cratonic areas such as the Kaapvaal Craton in southern Africa (Nair et al., 2006).

5. Conclusions

By applying a recently developed procedure to remove reverberations in P-to-S receiver functions caused by a low-velocity sedimentary layer, the petrological Moho and an intracrustal interface beneath the Williston Basin and adjacent areas with a sedimentary cover are revealed. The spatial correspondence between the thickness of the lower crustal layer and that of Phanerozoic sediments suggests that continuous density-increasing metamorphic reactions in the lower crustal layer played an important role in the long-term subsidence of the basin. An increase in lower crustal density through eclogitization or garnet growth, which was probably induced by continuous cooling of the crust that was greatly thickened by the Proterozoic collision between the Wyoming and Superior cratons, is a plausible cause of the increased crustal density, and consequently the ultimate mechanism for the formation and evolution of the Williston Basin.

CRediT authorship contribution statement

J. Song: Conducted the measurements, wrote part of the article while he was a visiting scholar at Missouri S&T.

S.S. Gao: Initiated and directed the project (with K. Liu), wrote part of the article, provided funding.

K.H. Liu: Initiated the project (with S.S. Gao), provided input and funding.

M. Sun: Worked with J. Song on data analysis.

Y. Yu: Major developer of the reverberation removal technique, produced Fig. S2.

F. Kong: Helped J. Song on data analysis, provided input on interpretation of results.

K. Mickus: Participated in the writing of the paper (especially the geological interpretation parts).

Declaration of competing interest

The authors declare that they have no known competing financial interests or personal relationships that could have appeared to influence the work reported in this paper.

Data availability

Data used in the study were obtained from the IRIS DMC and are publicly accessible from the IRIS DMC (https://ds.iris.edu/ds/nodes/dmc; last accessed: 03/2022). The data were from the following seismic networks: https://doi.org/10.7914/SN/CN; https://doi.org/10.7914/SN/IU; https://doi.org/10.7914/SN/N4; https://doi.org/10.7914/SN/TA; https://doi.org/10.7914/SN/US; https://doi.org/10.7914/SN/WY; https://doi.org/10.7914/SN/X6_2014; https://doi.org/10.7914/SN/XC_2000; https://doi.org/10.7914/SN/XI_2011; https://doi.org/10.7914/SN/XR_2001; https://doi.org/10.7914/SN/XS_1999; https://doi.org/10.7914/SN/XV_2009; https://doi.org/10.7914/SN/YB_1996.

Acknowledgements

We thank Editor Hans Thybo, reviewer Andrew Frederiksen, and an anonymous reviewer for constructive reviews that significantly improved the paper.

Most of the seismic data were from the TA network and were made freely available as part of the EarthScope USArray facility, operated by IRIS and supported by the National Science Foundation, under Cooperative Agreement EAR-1261681. J.S. was supported by a National Natural Science Foundation of China project titled Prestack Data Mining and Nonlinear Reservoir Parameter Prediction (No. 41674125) and a project titled Deep-Superdeep Oil and Gas Geophysical Exploration (B18055), S.G. was supported by United States National Science Foundation award 1919789, and K.L. and S.G. were supported by the American Chemical Society Petroleum Research Fund under awards 55903-ND8 and 60281-ND8, respectively.

Appendix A. Supplementary material

Supplementary material related to this article can be found online at https://doi.org/10.1016/j.epsl.2022.117686.

References

Allen, P.A., Armitage, J.J., 2012. Cratonic basins. In: Busby, C., Azor, A. (Eds.), Tectonics of Sedimentary Basins: Recent Advances. John Wiley & Sons, Ltd, Chichester, UK.

Ammon, C.J., 1991. The isolation of receiver effects from teleseismic P-waveforms. Bull. Seismol. Soc. Am. 81 (6), 2504–2510.

Armitage, J.J., Allen, P.A., 2010. Cratonic basins and the long-term subsidence history of continental interiors. J. Geol. Soc. (Lond.) 167 (1), 61–70. https://doi.org/10.1144/0016-76492009-108.

Artyushkov, E.V., Baer, M.A., 1983. Mechanism of continental crust subsidence in fold belts: the Urals, Appalachians and Scandinavian Caledonides. Tectonophysics 100, 5–42.

Baird, D.J., Knapp, J.H., Steer, D.N., Brown, L.D., Nelson, K.D., 1995. Upper-mantle reflectivity beneath the Williston Basin, phase-change Moho, and the origin of intracratonic basins. Geology. https://doi.org/10.1130/0091-7613(1995)023<0431:UMRBTW>2.3.CO;2.

Bascou, J., Barruol, G., Vauchez, A., Mainprice, D., Egydio-Silva, M., 2001. EBSD-measured lattice-preferred orientations and seismic properties of eclogites. Tectonophysics 342, 61–80.

Beaumont, C., 1978. The evolution of sedimentary basins on a viscoelastic lithosphere: theory and examples. Geophys. J. R. Astron. Soc. 55 (2), 471–497.

Benz, H.M., Vidale, J.E., 1993. Sharpness of upper-mantle discontinuities determined from high-frequency reflections. Nature 365, 147–150. https://doi.org/10.1038/365147a0.

Bollmann, T.A., van der Lee, S., Frederiksen, A., Wolin, E., Revenaugh, J.S., Wiens, D., Darbyshire, F.A., Stein, S., Wysession, M.E., Jurdy, D., 2019. P wave teleseismic traveltime tomography of the North American Midcontinent. J. Geophys. Res., Solid Earth 124, 1725–1742. https://doi.org/10.1029/2018JB016627.

Bostock, M.G., 1999. Seismic waves converted from velocity gradient anomalies in the Earth's upper mantle. Geophys. J. Int. 138 (3), 747–756. https://doi.org/10.1046/j.1365-246x.1999.00902.x.

Bousquet, R., Goffe, B., Henry, P., Le Pichon, X., Chopin, C., 1997. Kinematic, thermal and petrological model of the Central Alps; Lepontine metamorphism in the upper crust and eclogitisation of the lower crust. Tectonophysics 273 (1–2), 105–127.

Burgess, P., 2008. Phanerozoic evolution of the sedimentary cover of the North American Craton. In: Miall, A.D. (Ed.), Sedimentary Basins of the World, vol. 5. Oxford Press, Boston, USA, pp. 31–63.

Cox, R.T., Van Arsdale, R.B., 2002. The Mississippi Embayment, North America: a first order continental structure generated by the Cretaceous superplume mantle event. J. Geodyn. 34, 163–176. https://doi.org/10.1016/S0264-3707(02)00019-4.

Daly, M.C., Fuck, R.A., Julia, J., Macdonald, D.I.M., Watts, A.B., 2018. Cratonic basin formation: a case study of the Parnaiba Basin of Brazil. Geol. Soc. (Lond.) Spec. Publ. 472. https://doi.org/10.1144/SP472.20.

Dueker, K.G., Sheehan, A.F., 1997. Mantle discontinuity structure from midpoint stacks of converted P to S waves across the Yellowstone hotspot track. J. Geophys. Res. 102, 8313–8327.

Fischer, K.M., 2002. Waning buoyancy in the crustal roots of old mountains. Nature 417 (6892), 933–936. https://doi.org/10.1038/nature00855.

Foster, D.A., Mueller, P.A., Mogk, D.W., Wooden, J.L., Vogl, J., 2006. Proterozoic evolution of the western margin of the Wyoming craton: implications for the tectonic and magmatic evolution of the northern Rocky Mountains. Can. J. Earth Sci. 43, 1601–1619. https://doi.org/10.1139/E06-052.

Fowler, C.M.R., Nisbet, E.G., 1985. The subsidence of the Williston Basin. Can. J. Earth Sci. 22, 408–415.

Frederiksen, A.Q., Delaney, C., 2015. Deriving crustal properties from the P Coda without deconvolution: the southwestern Superior Province, North America. Geophys. J. Int. 201 (3), 1491–1506. https://doi.org/10.1093/gji/ggv086.

Gac, S., Huismans, R.S., Simon, N.S.C., Podladchikov, Y.Y., Faleide, J.I., 2013. Formation of intracratonic basins by lithospheric shortening and phase changes: a case study from the ultra-deep East Barents Sea basin. Terra Nova 25, 459–464. https://doi.org/10.1111/ter.12057.

Green, D.H., Ringwood, A.E., 1967. An experimental investigation of the gabbro to eclogite transformation and its petrological applications. Geochim. Cosmochim. Acta 31 (5), 767–833. https://doi.org/10.1016/S0016-7037(67)80031-0.

Green, A.G., Weber, W., Hajnal, Z., 1985. Evolution of Proterozoic terrains beneath the Williston Basin. Geology 13 (9), 624–628.

Hamdani, Y., Mareschal, J.C., Arkanihamed, J., 1994. Phase-change and thermal subsidence of the Williston Basin. Geophys. J. Int. 116 (3), 585–597. https://doi.org/10.1111/j.1365-246X.1994.tb03282.x.

Haxby, W.F., Turcotte, D.L., Bird, J.M., 1976. Thermal and mechanical evolution of the Michigan Basin. Tectonophysics 12 (c), 57–75.

Jarvis, G.T., McKenzie, D.P., 1980. Sedimentary basin formation with finite extension rates. Earth Planet. Sci. Lett. 48 (1), 42–52.

Kaus, B., Connolly, J., Podladchikov, Y., Schmalholz, S., 2005. Effect of mineral phase transitions on sedimentary basin subsidence and uplift. Earth Planet. Sci. Lett. 233 (1–2), 213–228. https://doi.org/10.1016/j.epsl.2005.01.032.

Kay, R.W., Kay, S.M., 1991. Creation and destruction of lower continental crust. Geol. Rundsch. 80 (2), 207–223.

Keller, G.R., 2013. The Moho of North America: a brief review focused on recent studies. Tectonophysics 609, 45–55. https://doi.org/10.1016/j.tecto.2013.07.031.

Kent, D., Christopher, J., 1994. Geological history of the Williston basin and Sweetgrass arch. In: Shetsen, I. (Ed.), Geological Atlas of the Western Canada Sedimentary Basin. Canadian Society of Petroleum Geologists, Calgary, CAN, pp. 421–429.

Kern, H., Gao, S., Jin, Z., Popp, T., Jin, S., 1999. Petrophysical studies on rocks from the Dabie ultrahigh-pressure (UHP) metamorphic belt, Central China: implications for the composition and delamination of the lower crust. Tectonophysics 301, 191–215.

Laske, G., Masters, G., 1997. A global digital map of sediment thickness. Eos Trans. AGU 78, F483.

Liu, K.H., Gao, S.S., 2010. Spatial variations of crustal characteristics beneath the Hoggar swell, Algeria, revealed by systematic analyses of receiver functions from a single seismic station. Geochem. Geophys. Geosyst. 11 (8). https://doi.org/10.1029/2010GC003091.

Mickus, K., 2007. Precambrian blocks and orogen boundaries in the north-central United States determined from gravity and magnetic data. Geol. Soc. Amer. Mem. 200, 327–340. https://doi.org/10.1130/2007.1200(16).

Middleton, M.F., 1989. A model for the formation of intracratonic sag basins. Geophys. J. Int. 99 (3), 665–676.

Naimark, B.M., Ismail-Zadeh, T.A., 1995. Numerical models of a subsidence mechanism in intracratonic basins: application to North American basins. Geophys. J. Int. 123 (1), 149–160.

Nair, S.K., Gao, S.S., Liu, K.H., Silver, P.G., 2006. Southern African crustal evolution and composition: constraints from receiver function studies. J. Geophys. Res., Solid Earth 111 (2). https://doi.org/10.1029/2005JB003802.

O'Reilly, S.Y., Griffin, W.L., 2013. Moho vs crust-mantle boundary: evolution of an idea. Tectonophysics 609, 535–546. https://doi.org/10.1016/j.tecto.2012.12.031.

Quinlan, G., 1987. Models of subsidence mechanisms in intracratonic basins and their applicability to North American examples. In: Beaumont, C., Tankard, A.J. (Eds.), Sedimentary Basins and Basin-Forming Mechanisms, Calgary. In: Canadian Society of Petroleum Geologists, vol. 12, pp. 463–481

.

Randall, G., 1994. Efficient calculation of complete differential seismograms for laterally homogeneous earth models. Geophys. J. Int. 118 (1), 245–254. https://doi.org/10.1111/j.1365-246X.1994.tb04687.x.

Rumpfhuber, E.-M., Keller, G.R., 2009. An integrated analysis of controlled and passive source seismic data across an Archean-Proterozoic suture zone in the Rocky Mountains. J. Geophys. Res., Solid Earth 114 (8), B08305. https://doi.org/10.1029/2008JB005886.

Schmandt, B., Lin, F.-C., Karlstrom, K.E., 2015. Distinct crustal isostasy trends east and west of the Rocky Mountain Front. Geophys. Res. Lett. 42 (23), 10,290–10,298. https://doi.org/10.1002/2015GL066593.

Schulte-Pelkum, V., Mahan, K.H., Shen, W., Stachnik, J.C., 2017. The distribution and composition of high velocity lower crust across the continental U.S.: comparison of seismic and xenolith data and implications for lithospheric dynamics and history. Tectonics 36 (8), 1455–1496. https://doi.org/10.1002/2017TC004480.

Sears, J.W., Alt, D., 1992. Impact origin of large intracratonic basins, the stationary Proterozoic crust, and the transition to modern plate tectonics. In: Bartholomew, M.J., Hyndman, D.W., Mogk, D.W., Mason, R. (Eds.), Basement Tectonics 8: Characterization and Comparison of Ancient and Mesozoic Continental Margins. Kluwer Academic Publishers, Dordrecht, the Netherlands.

Shen, W., Ritzwoller, M.H., 2016. Crustal and uppermost mantle structure beneath the United States. J. Geophys. Res., Solid Earth 121 (6), 4306–4342. https://doi.org/10.1002/2016JB012887.

Sleep, N.H., Snell, N.S., 1976. Thermal contraction and flexure of Mid-continent and Atlantic marginal basins. Geophys. J. Int. 45 (1), 125–154.

Thurner, S., Margolis, R., Levander, A., Niu, F., 2015. PdS receiver function evidence for crustal scale thrusting, relic subduction, and mafic underplating in the Trans-Hudson Orogen and Yavapai province. Earth Planet. Sci. Lett. 426, 13–22.

Thybo, H., Nielsen, C., 2009. Magma-compensated crustal thinning in continental rift zones. Nature 457, 873–876. https://doi.org/10.1038/nature07688.

Watts, A.B., Tozer, B., Daly, M.C., Smith, J., 2018. A comparative study of the Parnaba, Michigan and Congo cratonic basins. In: Daly, M.C., Fuck, R.A., Julia, J., Macdonald, D.I.M., Watts, A.B. (Eds.), Cratonic Basin Formation: A Case Study of the Parnaba Basin of Brazil. Geol. Soc. (Lond.) Spec. Publ. 472. https://doi.org/10.1144/SP472.6.

Wittlinger, G.W., Farra, V., Hetenyi, G., Vergne, J., Nabelek, J., 2009. Seismic velocities in Southern Tibet lower crust: a receiver function approach for eclogite detection. Geophys. J. Int. 177, 1037–1049. https://doi.org/10.1111/j.1365-246X.2008.04084.x.

Yu, Y., Song, J., Liu, K.H., Gao, S.S., 2015. Determining crustal structure beneath seismic stations overlying a low-velocity sedimentary layer using receiver functions. J. Geophys. Res., Solid Earth 120 (5), 3208–3218. https://doi.org/10.1002/2014JB011610.

Zhang, H., van der Lee, S., Wolin, E., Bollmann, T.A., Revenaugh, J., Wiens, D.A., Frederiksen, A.W., Darbyshire, F.A., Aleqabi, G.I., Wysession, M.E., Stein, S., Jurdy, D.M., 2016. Distinct crustal structure of the North American Midcontinent Rift from P wave receiver functions. J. Geophys. Res., Solid Earth 121, 8136–8153. https://doi.org/10.1002/2016JB013244.